2012

On the Synthesis and Physical Properties of Iron Doped SnO2 Nanoparticles

X. Wei
University of Nebraska - Lincoln

R. Georgescu

N. Ali

I. Morjan

T. A. George
University of Nebraska - Lincoln

See next page for additional authors

Journal of
Nanoscience and Nanotechnology
Vol. 12, 9299–9301, 2012

On the Synthesis and Physical Properties of Iron Doped SnO_2 Nanoparticles

X. Wei[1], R. Georgescu[2], N. Ali[3], I. Morjan[2], T. A. George[1], F. Dumitrache[2], R. Birjega[2], M. Chipara[4,*], R. Skomski[1], and D. J. Sellmyer[1]

[1] Department of Physics and Astronomy, University of Nebraska, Lincoln, Nebraska, 68588, USA
[2] National Institute for Lasers, Plasma and Radiation Physics, Laser Department, Bucharest, Atomistilor 409, P.O. Box-MG-36, Romania
[3] CNC Coatings, Rochdale, England
[4] University of Texas Pan American, Department of Physics and Geology, Edinburg, Texas, 78541, USA

RESEARCH ARTICLE

The synthesis of iron doped tin oxide by pulsed laser pyrolysis is reported. The as obtained nanoparticles have a dominant SnO_2 phase (as revealed by Wide Angle X-ray Scattering), with particles of the order of 10 nm. The doping with iron or iron oxide triggers magnetic properties as confirmed by SQUID experiments. EDX measurements supported the presence of Fe while Wide Angle X-ray Scattering failed to sense any iron or iron-oxide phase. It is concluded that Fe is well dispersed within the tin-oxide nanoparticles. The coercitive field has a complex dependence on the Fe/Sn content suggesting that the magnetization is not controlled solely by the amount of Fe dispersed within the nanoparticles.

Keywords: Iron-Doped Tin Oxide, Laser Pyrolysis Synthesis, Magnetic Properties, Blocking Temperature, WAXS, TEM.

1. INTRODUCTION

In recent years, tin-oxide based nanomaterials have been investigated for potential applications in the harvesting of the energy of sun (actually indium tin-oxide[1]), new lithium-ion batteries,[2] and hydrogen photo-production or sensor applications.[3] Due to finite size effects, nanomaterials display properties that are distinct from the corresponding bulk alloys. Nanoparticles of tin-iron oxides with different stoichiometry have been obtained either by mechanical alloying (such as milling) of tin oxide with iron oxides[4]), chemical synthesis (precipitation exchange method[5]), or more recently by pulsed laser deposition,[6] sol–gel techniques,[7] or pulsed laser pyrolysis.[8]. Tin (IV) oxide, tin dioxide, or stannic oxide (SnO_2) is an oxygen deficient n-type semiconductor with a forbidden gap of 3.6 eV, and a tetragonal (rutile like) crystalline structure. Cassiterite is the mineral form of SnO_2. Tin (II) oxide or stannous oxide (SnO) is a semiconductor with a forbidden gap ranging between 2.5 eV and 3.0 eV characterized by a tetragonal crystalline structure analogous to PbO. Tin-iron oxide or tin ferrite nanoparticles are combining the tin oxide semiconducting features with the magnetic characteristics of iron and iron oxides. $SnFeO_2$ is a typical diluted magnetic semiconductor. At the other extreme, thin films of $SnFe_2O_4$ are semiconducting ferromagnetic materials with a band gap of about 2.6 eV at room temperature.[6] Mossbauer studies revealed three different sites of Fe ions within the SnO_2 lattice[7] and reported a complex behavior of the magnetization. From the magnetic point of view, tin-iron oxides belong to the class of diluted magnetic semiconductors; in this case, the Sn^{4+} ion is replaced by the smaller Fe^{3+} ion simultaneously with a weak shrinkage of the SnO_2 lattice.[8] Even more, the magnetic properties of oxides and in particular the magnetic properties of defected magnetic oxides is under investigation.[9–10]

2. EXPERIMENTAL METHODS

$Sn_{1-x}Fe_xO_2$ nanoparticles with various ratios between Fe and Sn were synthesized by pulsed laser pyrolysis.[9] The laser was operating at 1060 nm at a nominal power of 400 W. Gas phase precursors were $Sn(CH_3)_4$ and $Fe(CO)_5$. Air has been used as an oxidizing agent and C_2H_4 as laser light absorber. The temperature within the reaction chamber was ranging between 600 and 650 °C. Nanoparticles of tin oxide containing various amounts of iron or iron oxide have been synthesized by pulsed laser pyrolysis by adjusting the flow of $Fe(CO)_5$. The samples have been labeled

*Author to whom correspondence should be addressed.

1533-4880/2012/12/9299/003 doi:10.1166/jnn.2012.6784

Table I. Atomic composition of tin oxide-Fe nanoparticles.

	EDX measurements [at%]						
Sample label	C	O	Sn	Fe	Sn/O	C/(Sn+Fe)	Fe/Sn
SnO	0	50	50	0	1.0		0
SnO2	0	66	33	0	0.50	0	0
SnOFe-2	12.18	55.54	31.12	1.16	0.56	0.37	0.04
SnOFe-6	11.77	58.14	27.62	2.46	0.47	0.42	0.08
SnOFe-8	15.10	57.09	21.39	6.41	0.11	0.37	0.39
SnOFe-10	14.65	57.91	21.20	6.24	0.10	0.36	0.29

as SnOFe-2, SnOFe-4, SnOFe-6, SnOFe-8, and SnOFe-10 and contain various amounts of iron.

The crystalline structure of pristine and Fe-doped tin oxide nanoparticles has been characterized by Wide Angle X-ray diffraction by using a Bruker Discovery 8 spectrometer. The atomic composition of the as obtained samples was determined by X-rays energy dispersive analysis (EDX). Additional information about the morphology, size, and particle distribution of these samples has been obtained by transmission electron microscopy (TEM), high-resolution electron microscopy (HREM), and selected area electron diffraction (SAED). The magnetic properties of iron doped tin oxide nanocomposites were measured by Squid measurements performed at various temperatures ranging from 10 K to room temperature.

3. EXPERIMENTAL RESULTS AND DISCUSSIONS

EDX measurements were performed in order to assess the concentration of Fe in the SnO_2. Table I collects details about the atomic composition of the samples investigated, including the Fe/Sn ratio. As noticed from Table I, Fe ions have been successfully incorporated within the tin oxide.

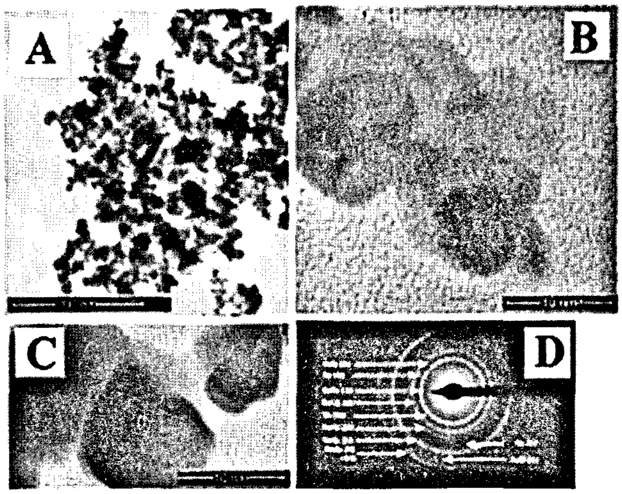

Fig. 1. Transmission Electron Microscopy photos of $SnOFe_6$ sample, characterized by a Fe/Sn ratio of about 0.08 (Figs. 1(A and B)) and of $SnOFe_2$ sample characterized by a Fe/Sn ratio of about 0.04 (Fig. 1(C)). Figure 1(D) shows the SAED spectrum of $SnOFe_2$ sample.

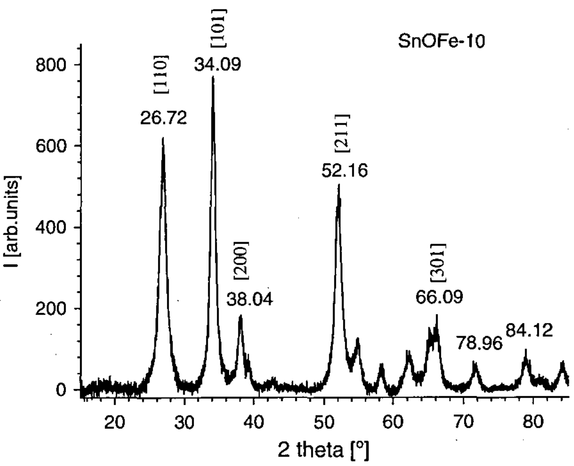

Fig. 2. Wide Angle X-Ray Scattering of $SnOFe_{10}$ nanoparticles showing the coexistence of three Sn related phases; metallic Sn (JCPDS 04-0673), SnO or romarchite (JCPDS 06-0395) and SnO_2 or cassiterite (JCPDS 41-1445). Indexed reflections indicate the SnO_2 phase, which is dominant.

The table reveals that some C has been incorporated also within the nanoparticles and suggests the possibility of oxygen vacancies in the as prepared samples.

The as obtained iron doped tin oxide particles have an average size of the order of 10 nm. Figure 1 shows, for example, the Transmission Electron Microscopy photos of SnOFe-6 sample, characterized by a Fe/Sn ratio of about 0.08 (Figs. 1(A) and (B)) and of SnOFe-2 sample characterized by a Fe/Sn ratio of about 0.04 (Fig. 1(C)). Figure 1(D) shows the SAED spectrum of SnOFe-2 sample. It is noticed that the nanoparticles are well crystallized and almost randomly oriented. The presence of metallic tin and tin-oxide (both SnO and SnO_2) is inferred from Figure 1(D).

Wide Angle X-ray Scattering (WAXS) of iron doped tin-oxide nanoparticles confirms the coexistence of three Sn related phases; metallic Sn (JCPDS 04-0673), SnO

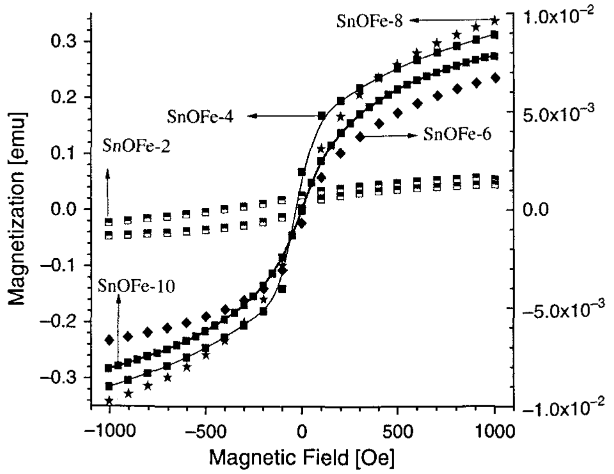

Fig. 3. The magnetization curves (magnetic moment versus the applied magnetic field for various $Sn_{1-x}Fe_xO_2$ nanoparticles.

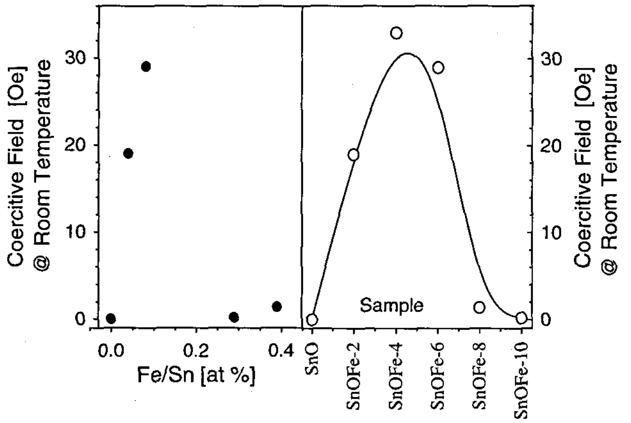

Fig. 4. The dependence of the coercitive field on the Fe/Sn ratio (left panel) or on composition of iron doped tin oxide (right panel) as shown in Table I.

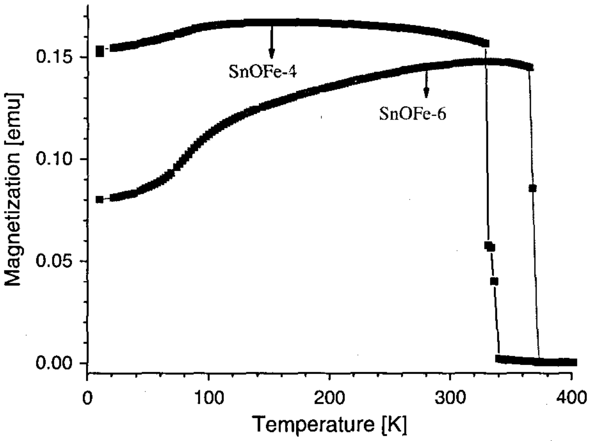

Fig. 5. The temperature dependence of the magnetization in Zero Field Cooling experiments for two iron doped tin-oxides.

or romarchite (JCPDS 06-0395) and SnO_2 or cassiterite (JCPDS 41-1445). The ratio between these three phases depends on the synthesis' details. Typically, the SnO_2 phase is dominant, as it is shown in Figure 2 for the sample SnOFe-10.

The average lattice parameters for a and c (for SnO_2) are ranging between 0.47 and 0.474 nm (for a) and respectively between 0.315 and 0.321 nm (for c). The doping by iron affects weakly the parameters of the crystalline lattice.

While the elemental analysis confirmed the presence of iron, WAXD data failed to notice an iron or iron-oxide phase. This suggested that the iron embedded within tin-oxide is very well dispersed. The presence of iron or iron oxides is supported by Squid measurements. Figure 3 shows the hysteresis loops for various iron doped tin oxide at room temperature. Excepting sample SnOFe-4, all other samples show weak magnetic features. The coercive field is expected to depend on the composition of the sample (iron content). However, the coercivity of these nanoparticles does not increase proportional to the concentration of Fe (or with the Fe/Sn ratio) as noticed from Figure 4. This suggests that other parameters such as the size of the crystalline lattice or the oxygen vacancies are competing to the overall magnetic properties of these nanocomposites.

The large differences between the magnetic properties of these samples are illustrated by Figure 5, where the ZFC dependencies have been represented for two samples. A large difference in the blocking temperature between the samples SnOFe-4 and SnOFe-6, with sample SnOFe-4 still magnetic at room temperature.

4. CONCLUSIONS

The synthesis of iron doped tin oxides by pulsed laser pyrolysis is reported. Both elemental and magnetic measurements investigations confirmed the presence of iron or iron oxide. WAXS and SAED measurements confirmed that the iron component is well dispersed within the tin oxide crystals. The complex dependence of magnetic properties on the Fe/Sn ratio may reveal the role of oxygen vacancies or of combined iron/iron oxides dispersed phases on the magnetic properties of the as obtained nanocomposites.

Acknowledgments: This research has been supported by the CONTACT grant (Air Force Research Laboratory under agreement number FA8650-07-2-5061), by NSF-MRSEC (Grant No. DMR-0820521), and by NCMN.

References and Notes

1. H. Schmidt, H. Fluegge, T Winkler, T. Buelow, T. Riedl, and W. Kowalsky. *Applied Physics Letters* 94, 243302 **(2009)**.
2. F. Belliard, P. A. Connor, and J. T. S. Irvine, *Solid State Ionics* 135, 163 **(2000)**.
3. S. Shukla, S. Patil, S. C. Kuiry, Z. Rahman, T. Du, L. Ludwig, C. Parish, and S. Seal. *Sensors and Actuators B-Chemical* 96, 343 **(2003)**.
4. O. N. C. Uwakweh, R. P. Moyet, R. Mas, C. Morales, P. Vargas, J. Silva, Á. Rossa, and N. López, *Journal of Physics: Conference Series* 217, 1 **(2010)**.
5. L. Yanwu, O. Yiyu, and L. Fangxin, *Rare Metals* 25, 493 **(2006)**.
6. R. K. Gupta and F. Yakuphanoglu. *Journal of Alloys and Compounds* 509, 9523 **(2011)**.
7. K. Nomura, C. A. Barrero, J. Sakuma, and M. Takeda. *Phys. Rev. B* 75, 184411 **(2007)**.
8. R. Alexandrescu, I. Morjan, F. Dumitrache, R. Birjega, C. Fleaca, I. Soara, L. Gavrila, C. Luculescu, G. Prodan, V. Kuncser, and G. Filoti, *Applied Surface Science* 257, 5460 **(2011)**.
9. R. Skomski, X. H. Wei, B. Balamurugan, M. Chipara, and D. J. Sellmyer, *IEEE Transactions on Magnetics* 46, 2427 **(2010)**.
10. M. Scarisoreanu, I. Morjan, R. Alexandrescu, R. Birjega, I. Voicu, C. Fleaca, E. Popovici, I. Soare, L. Gavrila-Florescu, O. Cretu, V. Ciupina, and E. Figgemeier, *Appl. Surf. Sci.* 253, 7908 **(2007)**.

Received: 1 January 2012. Accepted: 15 June 2012.

RESEARCH ARTICLE